Noncontact techniques for monitoring of tunnel linings

Joshua White[*1,2], Stefan Hurlebaus[1,2], Parisa Shokouhi[3], Andreas Wittwer[4] and Andrew Wimsatt[2]

[1]*Zachry Department of Civil Engineering, Texas A&M University, 3136 TAMU, College Station, TX 77843, USA*
[2]*Texas A&M Transportation Institute, Texas A&M University System, 3135 TAMU, College Station, TX 77843, USA*
[3]*Federal Institute for Material Research and Testing (BAM), Unter den Eichen 87, 12205 Berlin, Germany*
[4]*SPACETEC Datengewinnung GmbH, Salzstraße 47, 79098 Freiburg, Germany*

Abstract.   An investigation of tunnel linings is performed at two tunnels in the US using complimentary noncontact techniques: air-coupled ground penetrating radar (GPR), and a vehicle-mounted scanning system (SPACETEC) that combines laser, visual, and infrared thermography scanning methods. This paper shows that a combination of such techniques can maximize inspection coverage in a comprehensive and efficient manner. Since ground-truth is typically not available in public tunnel field evaluations, the noncontact techniques used are compared with two reliable in-depth contact nondestructive testing methods: ground-coupled GPR and ultrasonic tomography. The noncontact techniques are used to identify and locate the reinforcement mesh, structural steel ribs, internal layer interfaces, shallow delamination, and tile debonding. It is shown that this combination of methods can be used synergistically to provide tunnel owners with a comprehensive and efficient approach for monitoring tunnel lining conditions.

Keywords: ground penetrating radar; infrared thermography; structural health monitoring; ultrasonic tomography; nondestructive testing; tunnel lining

1. Introduction

During the 1960s and 1970s, the Interstate Highway System in the US reached its construction peak. This massive transportation undertaking resulted in almost 48 km of Interstate Highway tunnels built from coast to coast, which makes up over 40% of the total length of tunnels in the US (Abramson and MacDonald 2006). The nation's infrastructure is aging, and with some of these tunnels now over 50 years old, preventive maintenance safety measures require tunnel owners to thoroughly and routinely inspect tunnel linings. No mandatory tunnel inspection guidelines currently exist as do guidelines for highway bridges, but a scan team sponsored by the National Cooperative Highway Research Program (NCHRP), American Association of State Highway and Transportation Officials (AASHTO), and the Federal Highway Administration (FHWA) recommends a required tunnel inspection frequency that is applicable to all tunnels (FHWA 2012).

∗Corresponding author, E-mail: joshwhite@tamu.edu

Routine monitoring of tunnels to ensure optimal structural health is critical for early detection of damage that could potentially lead to safety hazards.

Tunnel owners employ a wide range of inspection procedures for routine tunnel lining monitoring. The decision to take action to repair a defected lining is typically the result of such maintenance evaluations. The primary inspection method, visual inspection, is often the only tool used to determine areas requiring attention and consists of noting areas of possible concern and recording their growth and effects over time (Sandrone and Wissler 2011). Inspectors are trained to keep detailed reports of the progression of damage.

There are, however, two distinct needs in monitoring a structure's health: comprehensive coverage and efficiency of inspection. Since typical evaluations only involve visual inspection, the first need is typically not met because distress observed is often the final result of underlying damage that has gone previously undetected by the naked eye. For this reason, noninvasive monitoring techniques are needed to complement visual inspection in order to detect the beginning stages of damage before it inhibits serviceability requirements, or worse, becomes a public safety issue. Nevertheless, visual inspection is one of the most efficient inspection techniques, requiring only experience and proper certification. It is necessary then to identify and develop techniques with comprehensive coverage that can also scan linings efficiently (minimizing inspection time and cost). When these early stages are identified by nondestructive testing (NDT) methods before significant damage has taken place, preventive actions can be recommended that will arrest the development of further damage.

The objective of this paper is to (1) describe the implementation of a noncontact NDT technique (air-coupled GPR) and one noncontact technology (SPACETEC) in two field evaluations of public tunnels with different lining characteristics; (2) show the added value of using combinations of these methods (rather than individual ones) in addition to routine visual inspection at detecting and locating the reinforcement mesh, structural steel ribs, internal layer interfaces, delamination, and areas of tile-debonding; and (3) compare the noncontact results with an in-depth investigation using two contact techniques, ground-coupled GPR and ultrasonic tomography (UST).

2. NDT methods used in investigation

The following is a description of each NDT technique used in this study. The noncontact methods were chosen because of their high speed capabilities. Air-coupled GPR can rapidly scan areas, particularly those with restricted access such as the upper or lower air ducts. The laser/thermal scanning system used here can also be used to rapidly scan heavy-traffic areas, but with more coverage than a single GPR scan. The motivation behind using rapid techniques in the two tunnels presented here is that these tunnels are high-volume traffic areas with highly-constricted movement. This threatens automobile safety and emphasizes the need to make roadway scans as rapid as possible to minimize the costly and dangerous traffic disruption. Ground-coupled GPR and ultrasonic tomography techniques are chosen because of their previous use in other structural applications for identification of deterioration as described below.

2.1 Ground penetrating radar

GPR is primarily useful for locating subsurface defects during project evaluation as well as detecting and locating moisture in concrete that facilitates reinforcement corrosion (Saarenketo and Scullion 2000, Alongi *et al.* 1992). This technique works by sending discrete electromagnetic (EM) pulses into the structure and capturing the reflections from subsurface layer interfaces. According to the physical laws governing the reflection and transmission of EM waves in layered media, each interface within a structure reflects and transmits parts of the incident energy. The ratio of reflected to transmitted energy depends on the dielectric constant contrast of the materials on either side of the interface. Since normal-weight concrete typically has a dielectric value between 8 and 12, values above this range may indicate excessive moisture and values below this range indicate lower than normal material density (i.e., air voids). The surface dielectric was therefore used as an indication of potential moisture intrusion due to severe cracking and delamination.

Studies have shown GPR is highly effective when combined with other NDT methods (Kohl *et al.* 2005, Maierhofer *et al.* 2004, Cruz *et al.* 2010). The high-speed nature of GPR and its sensitivity to changes in surface dielectric makes it an ideal candidate to use with laser scanning. Areas within the tunnel with surface dielectric peaks or notable areas located by visual inspection were marked for further evaluation via ground-coupled GPR and UST.

GPR antennas can emit EM pulses of different frequencies. The choice of frequency depends on the required depth of penetration and depth resolution. In general, higher frequency antennas show better details of reflectors close to the surface, but do not penetrate as deep as the low frequency antennas. The choice of antenna is therefore task-dependent and must be made from the user's experience and availability of other NDT methods.

Two types of GPR systems are typically used in structural investigations: air-coupled (A.C.) systems and ground-coupled (G.C.) systems. Both types are used in this study and are described below.

2.1.1 High-speed A.C. GPR

The high-speed A.C. systems are excellent tools for network-level data collection capable of testing up to 100 km/hr with 610 mm penetration in some materials (Saarenketo and Scullion 2000). Since the tunnel plenums in this investigation are only accessible by foot, a 1 GHz center frequency antenna was mounted on a cart and wheeled throughout the entire length of the tunnel to inspect the linings within the plenum (Fig. 1(a)). For roadway inspection, the same antenna can be mounted on a vehicle to inspect the linings within the roadway.

2.1.2 Automated G.C. GPR

The G.C. GPR systems provide better depth penetration with higher densities of readings than the A.C. systems, therefore they are excellent for project-level data collection in locating steel and defects in concrete. In this study, a 1.5 GHz center frequency antenna was used. This antenna was mounted on an automated scanner developed by the Federal Institute for Materials Research and Testing (BAM) and is shown in Fig. 1(b). The scanner system (named the ZFP-Scanner) can be used on any degree of surface orientation, including overhead testing. The scanner is fixed to the testing surface using pneumatically-operated vacuum plates and allows testing speeds up to 14.5 m^2/hr. The maximum testing area covered by this scanner is 1.6 m^2, making the time for a single site evaluation approximately 7 minutes.
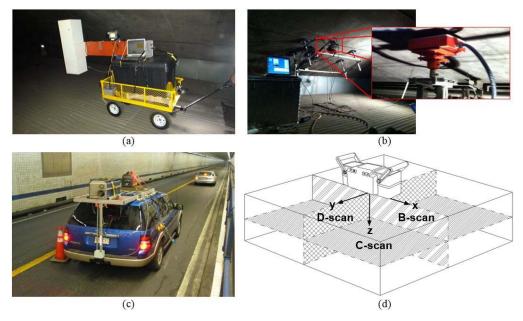
Joshua White et al.

Fig. 1 NDT equipment: (a) noncontact A.C. GPR on cart, (b) G.C. GPR on BAM ZFP-scanner, (c) noncontact vehicle-mounted SPACETEC equipment, and (d) UST with inspection planes

2.2 SPACETEC scanning system

The laser/thermal scanning system is a survey tool provided by SPACETEC (www.spacetec.de). Before this study this technology has not been used in the US, but laser scanning has been applied in European tunnel inspections (primarily railway) to aid in clearance checks and deformation profiling (Langer *et al.* 2000, Wang *et al.* 2009). The laser scanning system used here is a noncontact NDT technology that fuses visual, thermal, and spatial scanning data in a single measurement process. The system gathers information about the tunnel's geometry and surface condition by documenting all visible components, defects, and moist areas in a single image. The SPACETEC TS3 scanner (Fig. 1(c)) is a mature system developed specifically for the inspection of railway and roadway tunnels and records three different measurements in a single pass:

- Survey of the cross-sectional tunnel profile
- Full-surface visual recording of the tunnel lining
- Full-surface thermographic recording of the tunnel surface

The measurements are processed and can be viewed individually or together to detect and locate tunnel surface and near-surface anomalies. The high-resolution visual recording allows a thorough inspection of the tunnel surface and, combined with the profiling, the location of surface defects (Sandrone and Wissler 2011, Georg and Wiesler 1993).

Infrared thermography has continued to develop over the past few decades, becoming a highly useful technique well known for its capability of detecting superficial delaminations in concrete structures (Maser and Roddis 1990). Infrared technology is based on capturing thermal energy

emissions that escape all surfaces. The images produced give information concerning the temperature gradients observed. This is extremely convenient for NDT as delaminations and voids act as thermal barriers for heat released from concrete. However, it can be highly difficult to perform this testing, as infrared devices rely on stationary heat flow and therefore are extremely dependent on environmental conditions. Optimal results are obtained during the time of day when the temperature changes are more rapid. For the tunnel lining inspection, thermally cold spots in the images are usually indications of near-surface cavities or areas of moisture. Superimposing the thermal images on the visual recordings allows such zones to be easily detected and located.

2.3 Ultrasonic tomography

The ultrasonic system used here is a low-frequency device which incorporates a 4x12 array of dry point contact (DPC) transducers. This array uses mechanically isolated and dampened shear wave transducers, each with a center frequency of about 55 kHz. Low-frequency shear waves are used here because they carry more energy and are less prone to attenuation than longitudinal waves. The device fits the profile of a rough concrete testing surface with a variance of approximately 10 mm. Studies have shown ultrasonic technology to be applicable for measuring concrete member thickness (Acoustic Control Systems 2012), detection of grouting defects within tendon ducts (Friese and Wiggenhauser 2008, Krause *et al.* 2009, Im *et al.* 2010), determination of the extent of vertical surface cracks (Acoustic Control Systems 2012, Krause *et al.* 2009), crack repair quality assessment (Acoustic Control Systems 2012, Krause *et al.* 2009), detection of grouting defects behind railway tunnel linings (Acoustic Control Systems 2012), detection of honeycombing in concrete bridge decks (Acoustic Control Systems 2012), air- and water-filled voids in concrete (Wimsatt *et al.* 2013), abnormalities such as clay lumps (White *et al.* 2011), and the detection of delamination in concrete (Wimsatt *et al.* 2013, Shokouhi *et al.* 2011). The system used here represents an accumulation of the most recent developments in the ultrasonic NDT of concrete.

The UST system used here is the MIRA system produced by Acoustic Control Systems. Shear wave pulses are sequentially emitted by each block of 4 transducers and received by the remaining transducers in the array. Pulse reflections from internal interfaces where the material impedance changes are recorded, and with the help of a digitally focused algorithm (an alteration of the Synthetic Aperture Focusing Technique, or SAFT algorithm (Schickert *et al.* 2003)), a three-dimensional volume can be inspected after downloading the dataset on a laptop with reconstruction software. The volume under inspection is presented with each point of possible reflection in half-space represented by a color scheme and scaled according to reflecting power. This three-dimensional image can be dissected into each of the three planes representing its volume: the B-scan, C-scan, and D-scan (Fig. 1(d)). On each of the scans, the various intensities reported by the returned waves are color-coded from light blue to deep red, representing low reflectivity (typically sound concrete) and high reflectivity (any type of acoustic impedance contrast), respectively. With this intensity scaling, it is possible to see discontinuities with distinctly different wave speeds. The 48-transducer array is applied manually and data is collected by marking a user-defined scanning grid in increments related to the desired resolution. Typical testing time is dependent on the grid increments, but for comprehensive maps it can vary from 2.5-7 m^2/hr (Wimsatt *et al.* 2013). All UST testing in this study employs a 150 mm x 50 mm testing grid with shear waves emitted and received parallel to the length of the tunnel. The device is used here to further investigate areas isolated by the noncontact inspections. Since ground-truth

data is not typically available for verification, this robust UST system is used to validate potential areas of damage.

3. Descriptions of tunnels

Tunnel lining evaluations were performed in the following tunnels. The physical characteristics of each tunnel are given along with the methods used in the tunnel, followed by a section describing typical problems related to tunnel lining deterioration.

3.1 Eisenhower memorial tunnel

Eisenhower Memorial Tunnel, located approximately 97 km west of Denver, Colorado, is one of a 2.7 km twin bore tunnel started in 1968. The tunnel, which carries Interstate 70 west, is paired with the Edwin C. Johnson Memorial Tunnel which carries Eastbound I-70. Although the eastbound bore was not completed until almost 1980, construction on the Eisenhower bore was completed by 1973 after years of complicated tunneling techniques through numerous fault zones. Built using drill and blast methods, both tunnel bores transverse the Continental Divide (Fig. 2(a)). The maximum overburden is 448 m, and the average tunnel dimensions are 14.6 m in height and 12.2 m in width. Steel ribs were used as initial support prior to pumping in a cast-in-place concrete lining (Fig. 2(b)).

The Eisenhower Memorial Tunnel is a good representation of tunnels containing conventional reinforced concrete lining in addition to steel ribs as the initial tunnel support. Ribbed systems are typically a two-pass system for lining a drill-and-blast rock tunnel. The first pass consists of timber or steel ribs that usually contain blocking between them and against the ground. This provides structural stability to the tunnel. The second pass typically consists of poured concrete that is placed inside of the ribs.
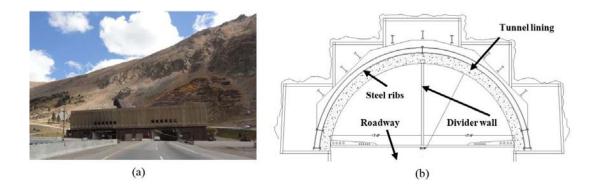

Fig. 2 Eisenhower Memorial Tunnel: (a) view of entrance and (b) view of the plenum
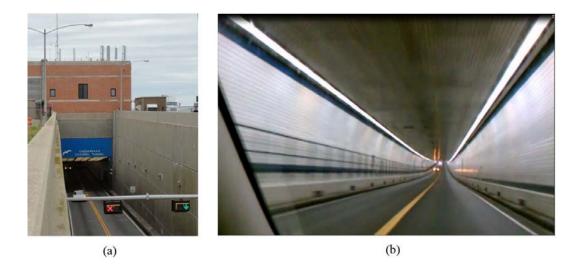
Fig. 3 Chesapeake Bay Tunnel: (a) view of entrance and (b) view of the roadway

3.2 Chesapeake bay tunnel

The Chesapeake Channel Tunnel (Fig. 3) is one of two tunnels that comprise the Chesapeake Bay Bridge Tunnel system, joining southeastern Virginia to the Delmarva Peninsula. Hailed worldwide as a modern engineering wonder, the 37 km system includes 3.2 km of causeway, four manmade islands, 8.9 km of approach roads, 19.3 km of low-level trestle, two 1.6 km steel-tubed tunnels, and two bridges. The Chesapeake Channel Tunnel was constructed using the immersed tube method. Precast steel tubes, fabricated and assembled in Orange, Texas, were floated to a shipyard in Norfolk, Virginia, where the reinforced concrete linings and roadway were constructed. The sections were floated to the site before being sunk into a trench. Each steel tube, 91 m in length and 11.3 m in diameter, was joined to its adjoining section and welded together. Patches between each section had to be formed with concrete to make an overlapping seal. Construction started in November 1960 and was opened to the public in April 1964.

3.3 Typical causes of tunnel lining deterioration

Corrosion of steel ribs and reinforcement may cause scaling or flaking and often results in heavy, stratified corrosion or in the worst case corrosion scaling with pitting of the metal surface. This corrosion condition eventually culminates in loss of steel section and generally occurs due to water infiltration. Since corrosion is accompanied by an increase in volume, if ribs are encased in shotcrete or concrete, cracking and spalling may occur. The concrete segments, which are applied as a final lining in Eisenhower Memorial Tunnel, are reinforced with steel bars. These are subject to corrosion if adequate concrete cover or positive corrosion protection is not provided.

Placed concrete sections within steel tubes (used in the construction of Chesapeake Channel Tunnel) are reinforced with steel bars and are subject to corrosion if adequate concrete cover or

positive corrosion protection is not provided (FWHA 2009). Chloride- and carbonation-induced corrosion is most common. Lack of water tightness in concrete lined tunnels may occur where inadequate provisions are made for sealing the joints between sections or where provisions for sealing have become defective. Defective grouting between the linings where sections tubes are joined promotes misalignment, which decreases gasket capacity and may allow water to seep through. The resulting moisture, particularly in cases involving dissolved salts, may cause chloride contamination of the concrete that causes electrolytic action with the steel reinforcement. This frequently results in corrosion and consequent cracking of the surrounding concrete, leading to spalling of the concrete and loss of structural capacity.
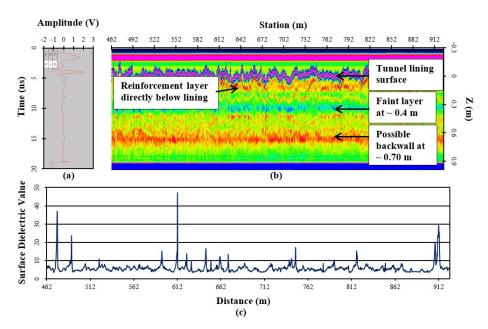

Fig. 4 GPR Data for Eisenhower Memorial Tunnel: (a) A-scan, (b) B-scan, and (c) surface dielectric

4. Field investigation

The following is a detailed description of the NDT testing conducted in the tunnels. In each tunnel, a combination of noncontact methods was used to evaluate the lining condition, and select areas of potential distress were further investigated by the more in-depth contact techniques for verification.

4.1 Eisenhower memorial tunnel investigation

The approach to evaluating the lining condition within the plenum consisted of first performing an A.C. GPR survey. In order to identify areas within the tunnel to test, the A.C. GPR was mounted on a cart and maneuvered through the plenum of the tunnel. The GPR output consists of radargrams which are a series of amplitude vs. time plots modified by the dielectric constant to

reveal depth (Figs. 4(a) and 4(b)). These radargrams and the surface dielectric are analyzed to determine lining thickness, general layer interfaces, and possible regions of distress that should be revisited with G.C. GPR and US techniques. The resulting radargram shows the tunnel lining surface as the primary high-amplitude response, along with multiple lower amplitude positive peaks corresponding to the closest layer of reinforcement (these areas are called out in Fig. 4(b)). Of particular interest in this investigation is a consistent region of negative amplitude peaks at an average 0.4 m below the surface. This negative amplitude occurs when the radar pulse goes from a layer of higher dielectric to a lower dielectric, and likely indicates a region of low density. This feature in the radargrams is investigated in the in-depth methods, and is shown to most likely be the structural steel ribs used during construction. The low-density signals revealed in the radargrams indicate the concrete-steel bonding may be compromised.

In addition to the radargrams, the significant local variations in surface dielectric (Fig. 4(c)) were used as an indication of potential moisture intrusion due to severe cracking and delamination. Also marked for further inspection were areas identified by visual inspection. Areas tested on the lining include representative locations of relatively sound (uncracked) concrete and areas with particularly extensive surface cracks and crazing in the tunnel lining, some with significant stalactite formation.

Once multiple areas of potential damage had been identified for inspection, these testing sites were further evaluated with more in-depth methods: the contact G.C. GPR and UST. Although multiple test sites were evaluated, only one is shown here as a representative of the chosen sites.

4.1.1 G.C. GPR application and results

A 1.0 m x 0.6 m test area, located 0.7 m east of a lining joint, is presented as a typical representation of the G.C. GPR scans (Fig. 5). The polarization of the G.C. GPR antenna was chosen parallel to the centerline of the tunnel.
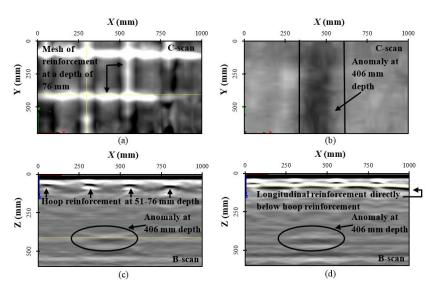

Fig. 5 GPR scan sets: (a)-(b) C-scans at two different locations, taken at 76 mm and 406 mm, respectively, and (c)-(d) B-scans at two different locations
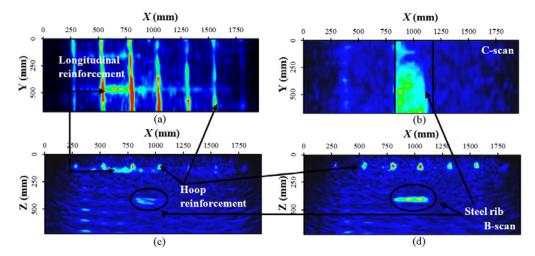
Fig. 6 UST scan sets: (a)-(b) C-scans at two different locations, taken at 105 mm and 409 mm, respectively, and (c)-(d) B-scans at two different locations

The testing increment for the evaluation was 51 mm. With the 1.5 GHz antenna, a rebar mesh at 51-76 mm from the surface was clearly detected with both the hoop and longitudinal reinforcement positioned regularly at 254 mm intervals (Fig. 5(a)). Moreover, an anomaly at 406 mm depth (the same depth as the low-density areas indicated in the radargrams) was detected. The anomaly has a horizontal width of 254 mm and runs along the entire vertical distance of the test area. C-scans showing the reinforcement bars and the anomaly at their respective depths are shown in Figs. 5(b)-5(d).

4.1.2 UST verification and results

Fig. 6 shows the results of a UST scan around a selected test site. The hoop reinforcement is shown to be 104 mm in depth and at a spacing of 257 mm, with the longitudinal reinforcement directly beneath. The same anomaly detected by both GPR methods is shown to be approximately 409 mm deep and 343 mm wide. This anomaly was found to be consistently spaced and present in every test site, supporting the idea that it is part of the steel ribbed support system.

4.2 Chesapeake bay tunnel investigation

The testing procedure for Chesapeake Bay Tunnel involved scanning the tunnel using SPACETEC's laser and infrared sensors to first provide an overall evaluation, then using an in-depth method for investigation of areas of concern.

4.2.1 SPACETEC application and results

The survey was performed overnight. During the measurement, a sufficient temperature difference for a quasi-stationary heat flow was obtained. The TS3 scanner was installed on the roof in the rear part of the inspection vehicle shown in Fig. 1(c), which provided an undisturbed 360-degree measurement. The highest resolution of 10,000 pixels was used for an appropriate

imaging of fine-scale features (i.e., tile chipping). The vehicle should be driven smoothly through the tunnel without exceeding a target velocity to achieve optimal results. Since it was not always possible to maintain the target driving speed of 1.5 km/h with the employed inspection vehicle (temporary speeds of up to 3.5 km/h were sometimes necessary), some pixels were stretched in the driving direction. Driving too fast causes gaps of the laser scan lines at the tunnel wall, which influences in some cases visibility of the cracks.

For safety reasons, a full tunnel closure was not possible and the survey vehicle could not be driven in the middle of the tunnel to create one symmetric scan of the tunnel. As such, the tunnel was scanned two times; once driving the inspection vehicle in the north-south lane, and the other time, in the opposite south-north lane. This ensured high-quality data in both directions and no loss of data due to passing vehicles during the survey. The 360-degree display of the tunnel was projected with a defined scale onto a plane surface for a synchronous display of all three channels. Common features in the tunnel such as hand rails, air vents, and electrical and maintenance installations were identified as shown in Fig. 7. These include even the cemented cable conduits behind the ceramic tiles, which are only visible in the thermal image.
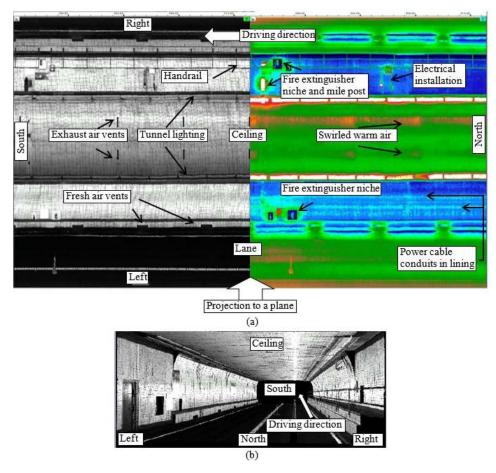

Fig. 7 (a) Typical features in SPACETEC survey data, and (b) 3D view of scan data which is calculated from survey data (not video data)

A full dataset consisted of a visual, thermal, and three-dimensional laser profile that was formatted and edited to evince a true-to-scale display, labeled with a distance range. The thermal data were corrected for the ambient air temperature drift along the tunnel axis by conducting a pre-measurement program which consisted of installing sensors in locations representing the tunnel's thermal activity. This provided the scan team with both an indication of the most ideal times for thermal measurements as well as typical temperatures differences for three zones: the air, 75 mm inside the lining, and 300 mm inside the lining. After ambient temperature corrections from real-time measurements taken during the scan, thermal data were displayed with a constant air temperature. This way, the same absolute color scale was used to describe the thermal variations everywhere in the tunnel. The data interpretation was based on local temperature differences.

Every thermographic surface point corresponded to a color-coded temperature interval with a resolution of 0.1 °C and 16 colors from black, blue, green, red, yellow, and white. This color palette gave an intuitive physiological impression of cold (dark to blue) and warm (red to white) areas.

Throughout the tunnel, thermal anomalies were detected and compared to the visual images to rule out system installations as a possible source. Thermal anomalies of unknown origin were marked for further investigation using in-depth techniques.

Fig. 8 shows a typical tunnel section where large thermal anomalies were detected. Two areas in particular (outlined in green in Fig. 8(a)) were inspected visually and by using hammer tapping. After hammer tapping Area I, it was clear by the audible low "pinging" that an area the size of the region shown in the thermograph contained debonded tiles. The tiles in Area II, however, did not appear to be debonded via hammer tapping.
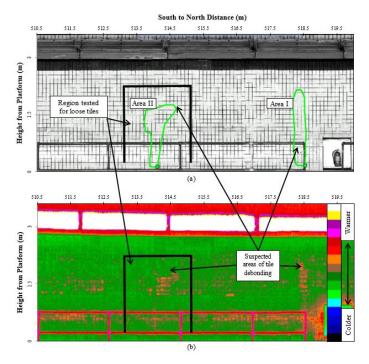

Fig. 8 SPACETEC (a) visual and (b) thermal images indicating possible tile debonding

4.2.2 UST verification and results

The UST results from Area II are shown in Fig. 9. The B- and D-scans (Figs. 9(a) and 9(c)) indicate the backwall reflection varies between 714-787 mm. This variance can be seen in the D-scan which shows the curvature of the tube's skin. The actual backwall curvature is greater than this since the UST inspection plane s are reconstructed for a flat surface, and the real testing area is actually slightly curved.

A C-scan at a depth of 102 mm (Fig. 9(b)) is shown at the reinforcement layer revealing the outline of an anomaly, possibly a shallow delaminated area above the reinforcement mesh. This helps to explain why such thermal activity could not be verified by hammer tapping; a delamination at this depth would certainly be difficult to hear with the human ear. When compared to SPACETEC's infrared analysis, this outline correlates strongly with the anomaly discovered by the infrared scan. It appears there is significant delamination at the level of reinforcement and above, and this has not yet caused debonding of the tile. The B-scan (Fig. 9(c)) also shows a portion of the delamination near the surface, as well as a potential crack (directly left of the last hoop rebar on the right). The hoop and longitudinal reinforcement are both detectable at 122-239 mm below the surface at 297 mm on center (again, refer to the D-scan and the hoop reinforcement profile). The longitudinal reinforcement is seen but is hard to differentiate between actual longitudinal rebars and 51 mm-diameter electrical ducts that are present. If the transducer polarization was changed, this distinction could likely be made.
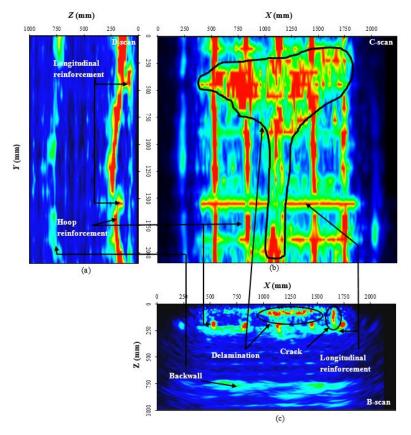

Fig. 9 UST scan sets of Area II: (a) D-scan, (b) C-scan, and (c) B-scan

5. Conclusions

The results of the two tunnel investigations indicate that the noncontact methods used here can add great value to the routine monitoring and inspections of the tunnel lining condition. Since the laser scanning technology cannot be easily used in areas of restricted access such as in the plenum, it is recommended to use A.C. GPR for high-speed surveys in these locations, and employ laser and thermal scanning on the roadway portion. This also ensures a rapid investigation in order to minimize traffic disruption.

Specifically, A.C. GPR surveys provide useful information for general nominal lining thickness and internal layers. The negative amplitudes in the radargrams identified potential debonding issues with the structural steel ribs that should be further investigated by ground truth data. In addition, the GPR survey provided information regarding changes in surface dielectric which can be related to moisture within the linings or possible voided areas. Surface dielectric changes were used to localize areas for in-depth inspection.

The G.C. GPR could provide a clear picture of the reinforcement mesh and deep (400 mm) anomalies detected by the A.C. GPR survey. The advantage of the G.C. GPR is that it can reveal clear images of the reinforcement mesh even in potentially delaminated regions, which is not possible with acoustic methods.

The SPACETEC technology was shown to provide detailed profile imaging for both visual and infrared analyses. Thermal profiles were investigated and anomalies that could not be explained by visual inspection were further inspected by UST to reveal internal delamination. The visual profile this technology provides presents another application of this system for routine inspections in monitoring the changes in the tunnel profile over time.

UST could clearly reveal the reinforcement mesh but could not detect any reinforcement directly below delaminated regions. UST also effectively revealed the presence of deep anomalies detected by the A.C. GPR survey. Since the UST method is very easy to apply manually, this anomaly wasdiscovered to exist at regular intervals, leading to the conclusion it was indeed the structural steel ribs used in construction.

Acknowledgments

References

Abramson, L. and MacDonald, H. (2006), "50 years of tunnels on the interstate highway system", *T. Res. E-Circular*, (E-C104), 96-108.
Acoustic Control Systems (2012), <http://acsys.ru/eng/production/?type_id=16&subtype_id=7&product_id =23>, Accessed November, 2012.
Alongi, T., Clemena, G. and Cady, P. (1992), *Condition evaluation of concrete bridges relative to reinforcement corrosion*, *SHRP Report*, SHRP-S/FR-92-105, **3**, Washington, DC.
Cruz, P.J.S., Topczewski, L., Fernandes, F.M., Trela, C. and Lourenco, P.B. (2010), "Application of radar techniques to the verification of design plans and the detection of defects in concrete bridges", *Struct.*

Infrastruct. E., **6**(4), 395-407.

Federal Highway Administration (2009), *Technical manual for design and construction of road tunnels-civil elements*, FHWA-NHI-10-034, Washington, D.C.

Federal Highway Administration (2012), *Innovations and best practices for roadway tunnels*, FOCUS, FHWA-HRT-12-012, Washington, DC.

Friese, M. and Wiggenhauser, H. (2008), "New NDT techniques for concrete elements: ultrasonic linear array and advanced imaging methods", *Proceedings of the International Conference of NDE/NDT for Highway and Bridges*, Structural Materials Technology (SMT), Oakland, CA, USA, Paper on CD-ROM.

Georg, A. and Wiesler, A. (1993), "Scanner-Aufnahmen der visuellen und Infrarot-Bild von Tunnelgewölben (Scanner Recordings of the Visual and Infrared Picture of Tunnel Vaults)", *Tunnel*, **5**, 256-268.

Im, S., Hurlebaus, S. and Trejo, D. (2010), "Inspection of voids in external tendons of posttensioned bridges", *Transportation Research Record: Journal of the Transportation Research Board*, (2172), Transportation Research Board of the National Academies, Washington, DC, 115-122.

Kohl, C., Krause, M., Maierhofer, C. and Wostmann, J. (2005), "2D- and 3D-visualisation of NDT-data using data fusion technique", *Mater. Struct.*, **38**(9), 817-826.

Krause, M., Gräfe, B., Mielentz, F., Milmann, B., Friese, M. and Wiggenhauser, H. (2009), "Ultrasonic imaging of post-tensioned concrete elements: new techniques for reliable localization of grouting defects", *Proceedings of the 2nd International Conference on Concrete Repair, Rehabilitation and RetrofittingII*, Cape Town, South Africa.

Langer, D., Mettenleiter, M., Härtl, F. and Fröhlich, C. (2000), "Imaging ladar for three-dimensional surveying and CAD modeling Of real world environments", *Int. J. Robot. Res.*, **19**(11), 1075-1088.

Maierhofer, C., Krause, M., Mielentz, F., Streicher, D., Milmann, B., Gardei, A., Kohl, C. and Wiggenhauser, H. (2004), "Complementary application of radar, impact-echo, and ultrasonics for testing concrete structures and metallic tendon ducts", *Transportation Research Record: Journal of the Transportation Research Board*, (1892), Transportation Research Board of the National Academies, Washington, DC, 170-177.

Maser, K.R. and Roddis, W.M.K. (1990), "Principles of thermography and radar for bridge deck assessment", *J. Transp. Eng. - ASCE*, **116**(5), 583-601.

Saarenketo, T. and Scullion, T. (2000), "Road evaluation with ground penetrating radar", *J. Appl. Geophys.*, **43**, 119-138.

Sandrone, F. and Wissler, R. (2011), "Laser scanning images analysis for tunnel inspection", *Proceedings of the 12th International Conference on Rock Mechanics of the International Society for Rock Mechanics*, Beijing, China.

Schickert, M., Krause, M. and Müller, W. (2003), "Ultrasonic imaging of concrete elements using reconstruction by synthetic aperture focusing technique", *J. Mater. Civil Eng.*, **15**(3).

Shokouhi, P., Wöstmann, J., Schneider, G., Milmann, B., Taffe, A. and Wiggenhauser, H. (2011), *Nondestructive detection of delamination in concrete slabs: multiple-method investigation*, Transportation Research Record: Journal of the Transportation Research Board, (2252), Transportation Research Board of the National Academies, Washington, DC, 103-113.

Wang, T.T., Jaw, J.J., Chang, Y.H. and Jeng, F.S. (2009), "Application and validation of profile-image method for measuring deformation of tunnel wall", *Tunn. Undergr. Sp. Tech.*, **24**(2), 136–147.

White, J., Hurlebaus, S., Scullion, T. and Wimsatt, A. (2011), "Detection of clay lumps in concrete using ultrasonic tomography", *Proceedings of the TRB 91st Annual Meeting*, Transportation Research Board of the National Academies, Washington, DC.

Wimsatt, A., White, J., Leung, C., Scullion, T., Hurlebaus, S., Zollinger, D., Grasley, Z., Nazarian, S., Azari, H., Yuan, D., Shokouhi, P. and Saarenketo, T. (2013), *Mapping voids, debonding, delaminations, moisture, and other defects behind or within tunnel linings*, SHRP 2 Final ReportS2-R06(G)-RW. Strategic Highway Research Program 2, Washington, D.C.